ACTA ACUSTICA UNITED WITH ACUSTICA
Vol. 91 (2005) 590 – 604

Wideband Measurement of the Acoustic Impedance of Tubular Objects

Maarten van Walstijn
Queen's University Belfast, Sonic Arts Research Centre, University Road, Belfast BT7 1NN, Northern Ireland

Murray Campbell, Jonathan Kemp
University of Edinburgh, School of Physics, King's Buildings, Mayfield Road, EH9 3JZ Edinburgh, Scotland

David Sharp
Department of Environmental and Mechanical Engineering, The Open University, Walton Hall, Milton Keynes, Bucks, MK7 6AA, United Kingdom

Summary
A method is discussed for measuring the acoustic impedance of tubular objects that gives accurate results for a wide range of frequencies. The apparatus that is employed is similar to that used in many previously developed methods; it consists of a cylindrical measurement duct fitted with several microphones, of which two are active in each measurement session, and a driver at one of its ends. The object under study is fitted at the other end. The impedance of the object is determined from the microphone signals obtained during excitation of the air inside the duct by the driver, and from three coefficients that are pre-determined using four calibration measurements with closed cylindrical tubes. The calibration procedure is based on the simple mathematical relationships between the impedances of the calibration tubes, and does not require knowledge of the propagation constant. Measurements with a cylindrical tube yield an estimate of the attenuation constant for plane waves, which is found to differ from the theoretical prediction by less than 1.4% in the frequency range $1\,\mathrm{kHz}$–$20\,\mathrm{kHz}$. Impedance measurements of objects with abrupt changes in diameter are found to be in good agreement with multimodal theory.

PACS no. 43.58.Bh, 43.75.Yy

1. Introduction

It is well known that the linear acoustic behaviour of tubular objects, such as pipes, horns, and cavities can be characterised by the acoustic response at the input end. Various methods have been devised to measure the response, usually defined in terms of planar mode acoustic impedance. Most of these methods involve the use of microphones, although other types of sensors have also been employed. A comprehensive review of techniques for measuring the acoustical response can be found in reference [1].

Besides experimental methods, the impedance can also be determined from theory, using a model that relates the geometry of the inner bore of a tubular object to its input impedance. In recent years, the experimental and theoretical approaches have been combined, with the objective of reconstructing bore profiles from measured response data. Development of this approach has resulted in accurate reconstructions of the bore profiles of a variety of tubular objects, including complex shapes such as musical wind instrument bores. Up to the present, such bore reconstructions have been achieved either by using the experimental time-domain technique of pulse reflectometry in combination with a fully inverted model [2, 3, 4], or with a frequency-domain method for measurement of the acoustic impedance in combination with a method for indirect inversion (i.e. optimisation) [5]. In both approaches, the geometry is derived from measured response data using a piecewise cylindrical section model in which only the planar mode of propagation is taken into account.

A major difficulty with either approach is to obtain a high axial resolution in the reconstructed profile. The axial resolution is largely determined by the frequency bandwidth used in the experimental determination of the acoustic response. In that respect, the problem of reconstruction of an internal bore profile from band-limited acoustic data is similar to the problem of reconstruction of a non-smooth time-domain signal from a truncated set of Fourier components. This limitation does not affect the reconstruction of smooth bore profile objects, but presents a significant problem when reconstructing any abrupt changes and discontinuities in diameter.

A second difficulty arises when attempting to reconstruct a tubular object in which the higher propagation modes are excited. Because the algorithms for bore reconstruction take into account only the planar mode, they are unreliable when applied to the reconstruction of an ob-

Received 25 June 2003, Revised 2 December 2004, accepted 5 May 2004.

ject in which the higher modes have a significant effect. This problem is in fact related to the bandwidth problem, because the higher modes are typically influential for short wavelengths. In addition, the higher modes are generally strongly excited at abrupt changes in the bore profile. Even though these modes may not be propagating throughout most of the air column, inter-mode coupling can still have significant effects on the planar mode response. In order to improve the precision of reconstructions of tubes with abrupt changes, the problems related to measurement bandwidth and those related to the higher-mode effects need to be addressed concurrently.

The aim of the present study is to develop techniques for accurate measurement of the impedance at higher frequencies than previously achieved, and to investigate to what extent the results obtained for objects with abrupt diameter changes are in agreement with multi-modal theory. A good match between theory and experiment is a prerequisite for the development of accurate reconstruction methods of such objects. The development of inverse modelling taking into account the higher-mode effects will be discussed in a future paper.

The method that is presented in this paper employs two microphones that monitor the air pressure in a cylindrical measurement duct (see Figure 1). The measurement duct is connected to a driver at one end and to the object under study at the other. The experiments are carried out at low amplitudes, such that the microphone signals are linear functions of pressure and volume velocity. The impedance of the object under study is derived from the ratio of the microphone signals, sometimes referred to as the "transfer-function" or the "standing-wave ratio". This is a well-known approach that has been applied to test impedances and reflection coefficients since the 1970s (see for example, [6, 7, 8, 9, 10, 11, 12, 13, 14, 15]). The relationship between the impedance and the microphone signal ratio can be expressed with a minimum of three complex coefficients. The majority of these methods are designed to measure of the absorption coefficient of materials, in which case sufficiently accurate results can be obtained using coefficients that are approximated by theory. However in application to measuring tubular objects, which typically have strong resonances and anti-resonances, it is necessary to determine these coefficients at each frequency via calibration [16].

As discussed by Dalmont [1], it is important to have an accurate analytical expression for the response of a calibration object, and for this reason closed tubes are often employed, rather than cavities or open-ended tubes. For a full calibration, three closed tubes of different lengths can be employed; this is the basic principle of the "Two-Microphone-Three-Calibration" (TMTC) method developed by Gibiat and Laloë [16]. The main disadvantage of this method is that the calculation of the impedance of closed tubes requires precise knowledge of the propagation constant, which is a frequency-dependent complex-valued parameter that depends on a number of air constants, such as the speed of sound, air density, and the viscosity coefficient. These constants are temperature-dependent, and it is usually difficult to obtain the precise set of constants for the environment in which the experiments take place.

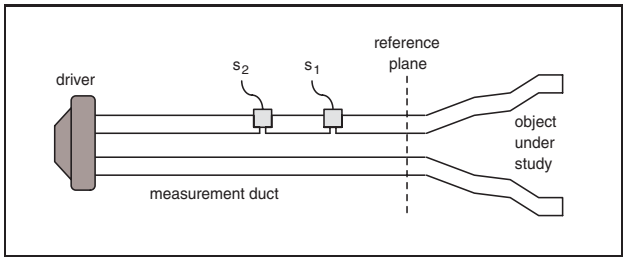

Figure 1. Sketch of the experimental set-up used in the TMFC method. The air inside the measurement head is excited using a compression driver. The impedance of the object connected to the measurement head is derived from the microphone signals s_1 and s_2.

There is a second, more fundamental reason for not using a calibration method in which accurate knowledge of the propagation constant is required. The accuracy of two-microphone techniques is typically tested by comparing theoretical and experimental results with a closed cylindrical tube of the same cross-section as the measurement duct, and usually of a greater length than the calibration tubes. The normalised impedance of such a tube contains exactly the same information as the propagation constant. For methods in which an analytical expression for the propagation constant has to be used in the calibration procedure, this is evidently not a valid method of verifying accuracy, since one has to first enter the same information that is to be measured.

Dalmont [17] has proposed an alternative method for calibration, which involves two calibration objects (a long and a short cylindrical tube, each with closed end). Direct calibration can only be carried out at the resonance frequencies of the long tube, the impedance at any other frequency being derived via interpolation. This method has been shown to be accurate for $ka < 1$, where $k = 2\pi f/c$ is the wave number, c is the wave velocity, and a is the radius of the tube measured. Dalmont used a tube of radius $a = 0.01$ m, and carried out measurements at frequencies up to 5 kHz. However, this method is not completely general; it relies on certain assumptions about the calibration coefficients and how these are affected by higher-mode effects, which increase with frequency. The accuracy of this calibration method at higher frequencies ($ka > 1$) has yet to be assessed.

In the present paper, a new calibration procedure is proposed, which involves the use of two microphones and four calibration measurements, and will therefore referred to as the "Two-Microphone-Four-Calibration" (TMFC) method. For a given, constant temperature, the TMFC method is completely general, and allows direct calibration and measurement at any frequency within a certain chosen bandwidth. Like the method of Dalmont, it does not require accurate knowledge of the propagation constant.

2. The Method

2.1. Theory

Wave propagation in acoustic tubes can be described by a set of propagation modes [4, 18, 19]. In the case of a cylindrical duct, all modes except the planar mode are evanescent below the cut-on frequency of the anti-symmetric (1,0) mode. For a cylindrical duct of radius a, this cut-on occurs at [18]:

$$ka = 1.84 \quad \text{or} \quad f = \frac{1.84c}{2\pi a}. \tag{1}$$

Propagation of planar waves is classically described using two variables, the value p of the pressure and the value U of the acoustical volume flow. The relationship between two sets of (p, U) spaced a distance L apart from each other along the longitudinal axis of a cylindrical duct can be defined using two complex-valued parameters, the propagation constant Γ and the characteristic impedance Z_c [20]:

$$p_1 = \cosh(\Gamma L)\, p_2 + Z_c \sinh(\Gamma L)\, U_2, \tag{2}$$
$$U_1 = Z_c^{-1} \sinh(\Gamma L)\, p_2 + \cosh(\Gamma L)\, U_2. \tag{3}$$

Both Z_c and Γ depend on the acoustical constants of the gas and on the duct diameter [21, 22].

The measurement duct depicted in Figure 1 has a cylindrical cross-section, with narrow and short side-branches at points where the microphones are fitted. Although an effort can be made to fit the microphones as flush as possible with the duct wall, it is in principal impossible to completely avoid the excitation of higher modes at these points, since this would require microphones with zero acoustic admittance. Hence there is inevitably some level of excitation of non-propagating modes at the positions of the microphones. Excitation of non-propagating modes will also occur at any non-cylindrical parts of the object under study; this includes cases where there is a diameter or taper discontinuity at the reference plane.

The experiments are carried out under the following conditions and assumptions. The air inside the measurement duct is excited only at frequencies below the cut-on frequency of the first higher mode. There is no significant coupling between any possible non-propagating modes at or beyond the reference plane and those excited at the microphone positions, because the distance between the reference plane and each of the microphones is significantly greater than the duct diameter. Finally, the oscillations in the duct are limited to the linear regime.

Under these conditions, the frequency components of the microphone signals s_1 and s_2 are linear functions of p and U at the reference plane:

$$s_1 = \alpha_1 p + \beta_1 Z_c U, \tag{4}$$
$$s_2 = \alpha_2 p + \beta_2 Z_c U, \tag{5}$$

where α_1, α_2, β_1, and β_2 are coefficients that depend on the manner in which waves propagate between microphones and the reference plane, as well as on the transducing characteristics of the microphones. The effects of non-propagating modes excited at the microphone positions are incorporated in these coefficients, although the exact values are not easily known from theory. The characteristic impedance Z_c has been put into these equations for mathematical convenience.

For passive terminations, one may define the impedance at the reference plane, which is the impedance load due to connecting the object to the measurement duct, as:

$$Z = \frac{p}{U}. \tag{6}$$

Following the general two-microphone approach, we define a new variable y as the ratio of the two microphone frequency-domain signals. From equations (4), (5) and (6), one then obtains:

$$y = \frac{s_2}{s_1} = \frac{\alpha_2 Z + \beta_2 Z_c}{\alpha_1 Z + \beta_1 Z_c}, \tag{7}$$

or

$$\bar{Z} = \frac{Z}{Z_c} = A\left(\frac{y - B}{y - C}\right), \tag{8}$$

with

$$A = -\beta_1/\alpha_1, \quad B = \beta_2/\beta_1, \quad C = \alpha_2/\alpha_1. \tag{9}$$

Equation (8) states that the normalised impedance (the ordinary impedance divided by the characteristic impedance of the measurement duct) of the object under study can be determined from a measured value of y and three coefficients A, B, and C. One possible approach is to approximate the values of these coefficients with theoretical expressions. However, as will be seen from the results presented in section 3.2, more accurate results are obtained via calibration.

For future reference, the response of the object under study may also be described as the ratio R of the backward- and forward-propagating planar mode waves at the reference plane, commonly known as the (planar mode) reflection coefficient. If no non-propagating modes are excited at the reference plane (i.e. if there is no cross-sectional or taper discontinuity at the reference plane), R is related to the normalised impedance by:

$$R = \frac{\bar{Z} - 1}{\bar{Z} + 1}. \tag{10}$$

2.2. Calibration

The impedance is derived from the knowledge of three pre-determined coefficients. Obtaining these coefficients via calibration amounts to carrying out various measurements with known reference impedances, and solving for the unknown coefficients from the equations that result from substituting the data in equation 8. Since we have three unknowns, three such equations are required. In the present study, these equations are deduced from measurements with four different reference impedances.

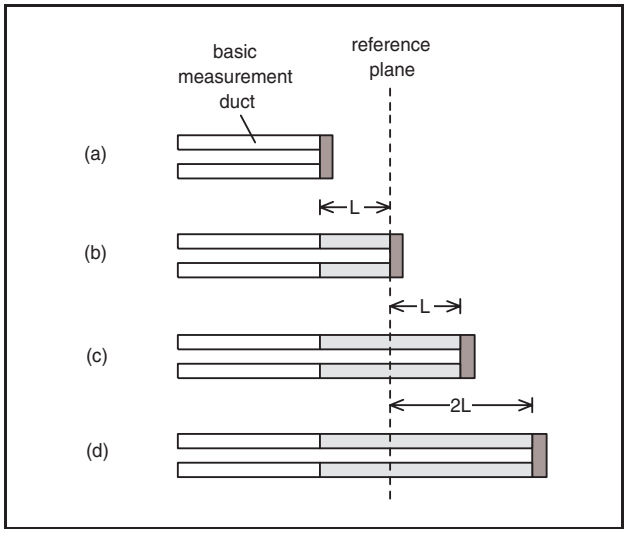

Figure 2. Bore configurations for the calibration measurements. (a) negative-length tube, realised by closing off the basic measurement duct. (b) Hard wall at the reference plane, realised by connecting a closed tube of length L to the basic measurement duct. (c) positive-length tube, realised by connecting a closed tube of length $2L$ to the basic measurement duct. (d) double-length tube, realised by connecting a tube of length $3L$ to the basic mea surement duct.

In the first calibration measurement, the duct is closed off at the reference plane, and the microphone ratio signal y_0 is measured. The hard wall that closes the duct off presents a zero-admittance termination[1]. In that case the denominator of the right-hand side of equation 8 must be zero, i.e.

$$C = y_0. \tag{11}$$

For the determination of coefficient B, two tubes of the same cross-section as the measurement duct, one of length L and one of length $-L$ are employed. The negative length can be realised by defining the position of the reference plane at a distance L from the basic measurement duct exit (see Figure 2). The microphone ratio signals measured with the positive- and negative-length tubes are y_p and y_n, respectively. The normalised planar mode impedance of a closed tube of length L is $\bar{Z} = \coth(\Gamma L)$. Since

$$\coth(-\Gamma L) = -\coth(\Gamma L), \tag{12}$$

we have

$$\bar{Z}_p + \bar{Z}_n = 0, \tag{13}$$

where $\bar{Z}_p$ and $\bar{Z}_n$ are the normalised impedances of the positive- and the negative-length tubes, respectively. Evaluation of the impedances in equation (13) using equation (8) gives

$$A\left[\left(\frac{y_p - B}{y_p - C}\right) + \left(\frac{y_n - B}{y_n - C}\right)\right] = 0. \tag{14}$$

After substitution of equation 11, the value of coefficient B is obtained as:

$$B = \frac{2y_p y_n - y_0\,(y_p + y_n)}{(y_p + y_n) - 2y_0}. \tag{15}$$

The value of B is equivalent to the microphone signal ratio that is obtained with an "ideal open end", i.e. a termination at the reference plane for which $Z = 0$ at all frequencies. Such an ideal open end can be simulated using an active termination [24], but a much better signal-to-noise ratio (SNR) can be obtained for coefficient B on the basis of equation 13.

For the determination of the coefficient A, another closed tube is connected to the measurement duct, this time of length $2L$, and the microphone ratio y_2 is measured. The reflection coefficient of a closed tube of length L is $R = \exp(-2\Gamma L)$, thus we have

$$R_2 = R_p^2, \tag{16}$$

where R_p and R_2 are the reflection coefficients of the closed tubes of length L and $2L$, respectively. Substitution of equation 10 yields:

$$\bar{Z}_p^2 - 2\bar{Z}_p\bar{Z}_2 + 1 = 0, \tag{17}$$

where $\bar{Z}_2$ denotes the normalised impedance of the double-length tube. After evaluation of the impedances $\bar{Z}_p$ and $\bar{Z}_2$ using equation 8, and substitution of equations 11 and 15, one obtains:

$$\begin{aligned} A^2 = &\left[\left(\frac{y_2 - y_0}{y_p - y_n}\right)(2y_0 - y_p - y_n)^2\right] \times \\ &[y_p y_2 + 3\,(y_p y_0 + y_2 y_n) \ldots \\ &-4\,(y_p y_n + y_2 y_0) + y_0 y_n]^{-1}. \end{aligned} \tag{18}$$

This equation has two roots. To find the correct value of A, both roots are substituted in equation 8 in order to compute the impedance $\bar{Z}_p$, and the corresponding two reflection coefficients are found with equation 10. When errors are small, one of the roots results in $|R_p| > 1$, the other in $|R_p| < 1$. The latter is the correct root. When errors are large, one also has to investigate the phase of the reflection coefficient.

Note that the correctness of the three assumptions upon which the calibration procedure relies, namely that equations 11, 13, and 16 are true, is independent of the value of the propagation constant. An important restriction is however that temperature fluctuations during the experiments should be avoided as much as possible, since the method assumes that Γ remains constant.

[1] The admittance is not strictly zero because of heat conduction at the wall [23]. The normalised admittance $\bar{Y}_t$ of the wall is extremely small; Dalmont [17] gives the value $\bar{Y}_t = 9.6 \times 10^{-6}\sqrt{f}(1 + j)$ at 20°C. Hence using $\bar{Y}_t = 0$ does not introduce any significant errors.

At first glance, it seems that the calibration length L can be chosen arbitrary. However, as is explained in section 2.3, this length should be chosen as half of the distance between the microphones in order to obtain the best results.

In various previous applications based on the two-microphone approach, in particular those applied to investigating sound-absorbing materials [6, 7, 8, 9, 10, 11, 12, 13, 14, 15], the values of the calibration coefficients are partly approximated by plane wave theory. In many cases, the influence of non-propagating modes is neglected, and the first microphone is assumed not to disturb the acoustical field. The coefficients in equations 4 and 5 can then be written:

$$\alpha_1 = H_1 \cosh(\Gamma x_1), \quad \beta_1 = H_1 \sinh(\Gamma x_1), \quad (19)$$

$$\alpha_2 = H_2 \cosh(\Gamma x_2), \quad \beta_2 = H_2 \sinh(\Gamma x_2), \quad (20)$$

where x_1 and x_2 are the positions of the microphones along the measurement duct, with $x = 0$ at the reference plane, and H_1 and H_2 are the microphone transducing characteristics. It follows from equations 9 that the calibration coefficients then are:

$$A = -\left[\frac{\sinh(\Gamma x_1)}{\cosh(\Gamma x_1)}\right], \quad (21)$$

$$B = G\left[\frac{\sinh(\Gamma x_2)}{\sinh(\Gamma x_1)}\right], \quad (22)$$

$$C = G\left[\frac{\cosh(\Gamma x_2)}{\cosh(\Gamma x_1)}\right], \quad (23)$$

where $G = H_2/H_1$. The above approximations are used with $G = 1$ in section 3.1 in order to predict the effects of noise and calibration errors, and are compared with experimentally derived values in section 3.2.

2.3. Errors and singularities

Any experimental procedure is subject to errors. Two kinds of error occur with the TMFC method, namely noise errors and calibration errors. Noise errors have a random character, and the exact way that this type of error appears in the measurement result is variable. The effect of noise errors depends on the method for excitation that is used; in general these effects can be largely reduced by carrying out the experiments in a quiet environment, and by averaging the measurement data.

Calibration errors are due to uncertainties in the knowledge of the impedances of the calibration objects, and are systematic errors that manifest themselves consistently in the same manner in the results. The calibration procedure described in section 2.2 does not depend on accurate knowledge of the propagation constant, nor on any other acoustical value or constant. It does strongly depend, however, on the accuracy of the lengths of the closed tubes, or more specifically, on the exactness of the ratios between the length of these tubes. That is, the correctness of equation 13 relies on the amount by which the measurement duct is effectively shortened being equal to the length of the positive-length tube, while the correctness of equation 16 relies on the assumption that y_2 is measured using a tube of a length that is exactly twice as long as the one used to measure y_p. Deviations in these tube length ratios will cause errors in the response, and for this reason, the calibration tubes must be manufactured with great precision[2].

The way in which the noise and calibration errors manifest themselves in the results depends on the geometry of the apparatus. A direct consequence of using two microphones is that any measurement errors (noise or calibration) are particularly strong at and around frequencies for which the distance d between the microphones equals half the wavelength (or one of its multiples), thus at frequencies

$$f = n \cdot \frac{c}{2d}, \quad (24)$$

for $(n = 1, 2, 3, ...)$. This effect occurs because at these frequencies, the signals s_1 and s_2 have exactly the same or opposite phase, and therefore they effectively provide the same information. In such cases, the system of equations from which the calibration coefficients are solved becomes singular. For this reason, these frequencies can be referred to as "singular frequencies" [25]. This phenomenon can be directly observed in the calibration method; when the phases of s_1 and s_2 are equal or opposite, the value of y is equal or close to either 1 or -1, regardless of the impedance load present at the reference plane. Therefore, both the denominator and numerator in equations 15 and 18 tend to zero, so that the coefficients B and A become ill-defined.

Singular frequencies also occur as a result of the dimensions of the calibration tubes. Whenever the tubes that are used for measuring the signals y_n and y_p both present a zero impedance load, these signals do not provide independent information, even though the condition in equation (13) is met. These singularities occur at

$$f = n \cdot \frac{c}{4L}, \quad (25)$$

for $(n = 1, 3, 5....)$. Further singularities occur when the two tubes that are used for determining coefficient A have nearly equal impedance loads (equal phase and marginally different magnitude), in which case the signals y_p and y_2 represent equivalent information. Singularities of this type occur at

$$f = n \cdot \frac{c}{2L}, \quad (26)$$

for $(n = 1, 2, 3, ...)$. It can be seen from equations 24, 25, and 26 that if we take $L = d/2$, the first singular frequency due to the calibration tube lengths coincides with the lowest singular frequency $f_c = c/(2d)$ due to the microphone distance. In order to ensure that the frequency

[2] In our experiments, the lengths of the calibration tubes were measured to be accurate within 0.02 mm.

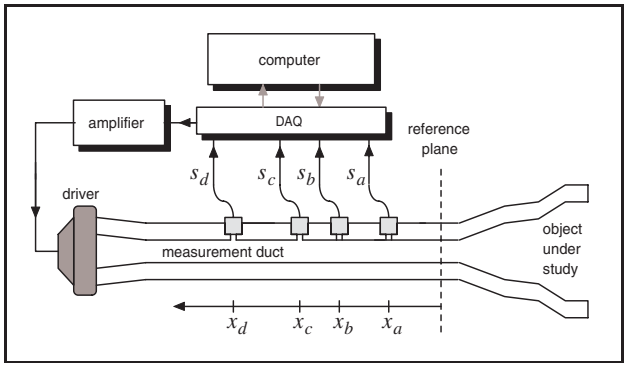

Figure 3. Schematic drawing of the experimental apparatus.

range $[0 - f_c]$ is free of singularities due to calibration tube dimensions, the basic calibration length L must be chosen no larger than $d/2$. Taking into account that $f = 0$ also forms a singularity, and that the effects of singularities are the strongest at and around singular frequencies [15, 25, 26], it follows that using $L = d/2$ is in fact the best choice in terms of creating a maximally wide band of frequencies within the frequency range $[0 - f_c]$ that is minimally affected by singularity effects.

It was found empirically that measurements with the TMFC method at frequencies larger than f_c tend to be less accurate than those within $[0 - f_c]$. As a consequence, no advantage can be gained by strategically combining the results obtained within the higher singularity-free areas ($[f_c - 2f_c]$, $[2f_c - 3f_c]$ etc.) of different microphone combinations, as done by Jang and Ih [26]. Hence the microphone distance should be chosen such that all frequencies to be measured are smaller than f_c. The effects that noise errors and calibration errors due to tube length uncertainties have on the results at frequencies in the range $[0 - f_c]$ can be predicted and analysed using computer simulations, and is discussed in section 3.1.

2.4. Apparatus

Figure 3 shows a schematic drawing of the experimental apparatus. The air inside the measurement duct and the object under study is brought into vibrational motion by the compression driver (type JBL 2426H), and the pressure in the duct can be measured at four different positions along the duct axis, using cylindrically-shaped microphones (type Sennheiser KE4-211) that are mounted in the duct wall. The distance x_a between the reference plane and the first microphone depends on the lengths of the calibration tubes. The other microphones are positioned at $x_b = x_a + 14\,\text{mm}$, $x_c = x_a + 21\,\text{mm}$, and $x_d = x_a + 49\,\text{mm}$. With these four microphones, measurements with six different microphone distances can be carried out (see Table I). Only two microphones are actively used per individual measurement session.

The microphone signals are sampled using a dynamic data acquisition card (National Instruments PCI 4451) and stored in computer memory. The excitation signal is calculated using the computer and converted into an analog signal with a second data acquisition card (National Instruments PCI 4452). The complex-valued frequency-domain descriptions of s_1 and s_2 are obtained by applying an FFT to the recorded microphone time-domain signals.

Table I. Possible microphone combinations in the experimental set-up and their measuring properties. BW is the measurement bandwidth. See text and Figure 3 for an explanation of the other quantaties.

combin.	s_1	s_2	d (mm)	f_c (kHz)	BW (kHz)
I	s_b	s_c	7	24.6	$7.4 - 20$
II	s_a	s_b	14	12.3	$3.7 - 10$
III	s_a	s_c	21	8.2	$2.4 - 6.7$
IV	s_c	s_d	28	6.1	$2.0 - 5.0$
V	s_b	s_d	35	4.9	$1.5 - 4.0$
vI	s_a	s_d	49	3.5	$1.0 - 2.9$

In order to obtain the required acoustic data for frequency f, a sinusoidal signal of that frequency is sent to the compression driver. This procedure is repeated for a series of frequencies. For each frequency, the length of the recorded microphone signal is chosen as an exact integer multiple of the period, such that the subsequent FFT analysis is free from numerical artefacts.

Experiments are carried out for a series of frequencies within a certain frequency band, without changing the settings of the amplifier. At the start of each measurement session, the amplitudes of the signals that are computed and sent to the driver are calibrated so that all frequencies have approximately equal amplitude at the microphones when the measurement duct is terminated anechoically. This is achieved by first measuring the microphone signals with a 30 m long tube connected to the measurement duct, using a set of driving signals with frequency-independent amplitude, and then adapting the amplitudes by dividing by $(|s_1| + |s_2|)/2$ and normalising. This procedure compensates for losses and resonance effects in the measurement duct, which is especially important for obtaining a good SNR at the higher frequencies. The sensitivity to noise errors is further reduced by averaging over a number of repeated periods in the microphone signals.

The radius of the measurement duct is $a = 4.9\,\text{mm}$. For temperatures above $20\,^o\text{C}$, the free-space sound velocity is larger than 343 m/s. It follows from equation 1 that all higher modes are evanescent in the measurement duct at frequencies below 20.5 kHz.

Empirically it was found that when using a microphone distance d, the effective measurement bandwidth within which accurate results can be obtained is approximately $[0.3 - 0.8]f_c$ (see also section 3.1). The effective bandwidths of the different possible microphone combinations of the experimental set-up are listed in Table I.

2.5. Discontinuity at the reference plane

The radius of the measurement duct is chosen such that for all frequencies below 20.5 kHz, any higher modes that are excited at the reference plane or within the object un-

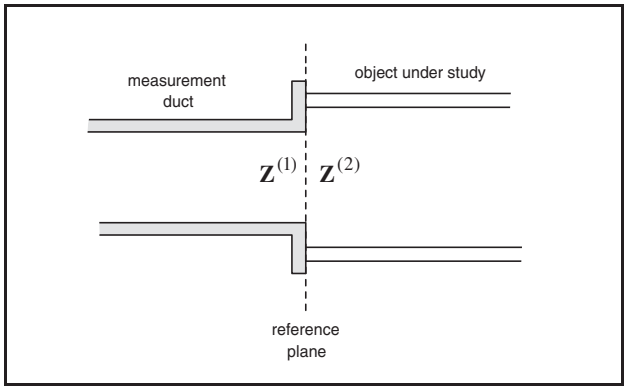

Figure 4. Discontinuity at the reference plane. $\mathbf{Z}^{(1)}$ is the impedance matrix as calculated on the left-hand side of the reference plane, the planar mode component of which is the impedance Z in equation 8. $\mathbf{Z}^{(2)}$ is the impedance matrix as calculated on the right-hand side of the reference plane, the planar mode component of which represents the impedance of the object under study.

der study do not propagate back to the microphones. However, in cases where non-propagating modes are excited at the reference plane, the impedance Z in equation 8 using the calibration procedure described in section 2.2 does not represent the planar mode impedance of the object. Instead it equals the planar mode impedance as calculated on the input side of the reference plane.

Figure 4 depicts a situation in which the object under study has an entry that is wider than the measurement duct; the cross-sectional discontinuity causes excitation of non-propagating modes at and around the reference plane. In order to clarify the relationship between the impedances on either side of the reference plane, the acoustic variables need to be written in multimodal form. Following recent studies in multi-modal modelling [4, 19], no anti-symmetric modes are taken into account, which is justified for discontinuities in axially symmetric structures. The pressure and volume velocity are denoted as the vectors $\mathbf{p}$ and $\mathbf{U}$, where the ith element of these vectors represents their ith axially symmetric mode component. The impedance is then defined as a matrix that relates the pressure to the volume velocity by

$$\mathbf{p} = \mathbf{Z}\mathbf{U}, \tag{27}$$

where the planar mode component is given by the corner-element $Z_{0,0}$. Referring to Figure 4, the impedance $\mathbf{Z}^{(1)}$ on the left side of the reference plane is related to the impedance $\mathbf{Z}^{(2)}$ by [19]:

$$\mathbf{Z}^{(1)} = \mathbf{F}\mathbf{Z}^{(2)}\mathbf{F}^{t}, \tag{28}$$

where $\mathbf{F}$ is a non-diagonal matrix that is defined by the boundary conditions at the walls of the tube at and around the discontinuity. It is shown in Appendix A2 that in cases where the non-propagating modes excited at the discontinuity are not coupled to any modes active within the rest of the object, the relationship between the planar mode components of the impedances on either side of reference plane can be derived from equation 28 as:

$$Z^{(2)}_{0,0} = Z^{(1)}_{0,0} - \sum_{n=1}^{N} (F_{0,n})^2 \, Z^{(c)}_{n,n}, \tag{29}$$

where $\mathbf{Z}^{(c)}$ is a diagonal matrix that represents the characteristic impedance on the right side of the discontinuity, and N is the number of higher modes taken into account. Thus, the planar mode impedance of an object that has a different diameter from the measurement duct can be derived from a measured value of the planar mode impedance on the left side of the reference plane using equation 29, provided that none of the non-propagating modes excited at the reference plane are coupled to any modes active in the remaining part of the object. In practice this means that the entry diameter must be less than twice the measurement duct diameter to avoid propagation of the axially symmetric $(0,1)$ mode within the entry region. The object must also have a cylindrical entry section of a length that is at least about twice its entry diameter, such that the non-propagating modes excited at the discontinuity are not coupled to any non-propagating modes in other parts of the object.

Furthermore the planar mode reflection coefficient must now be taken as the corner-element (i.e. $R_{0,0}$) of the reflection coefficient matrix, calculated as [4]:

$$\mathbf{R} = \left[\mathbf{Z}^{(2)}\left(\mathbf{Z}^{(c)}\right)^{-1} + \mathbf{I}\right]^{-1} \times \left[\mathbf{Z}^{(2)}\left(\mathbf{Z}^{(c)}\right)^{-1} - \mathbf{I}\right]. \tag{30}$$

There are however alternatives to the above approach. For example, Gibiat and Laloë [16] suggest the use of calibration tubes that have the same diameter as the object under study. The higher-mode effects are then automatically calibrated out. A practical disadvantage of this method is that many sets of calibration tubes are required to measure objects with a range of entry diameters.

If the main objective of the measurement is to use the data to reconstruct the bore profile of the object under study, it is sufficient to know the impedance on the measurement duct side of the reference plane. The discontinuity then forms a part of the reconstructed bore profile, and there is no need to know the actual planar mode impedance of the object as defined on the output side of the reference plane. In such applications, it is in fact advantageous to add a conical coupling section between the measurement duct and the object. This way, more acoustic energy can be injected into the object, which results in a better SNR.

3. Results

3.1. Error analysis via simulation

It is always useful to have knowledge of the manner in which errors manifest themselves in the measurement

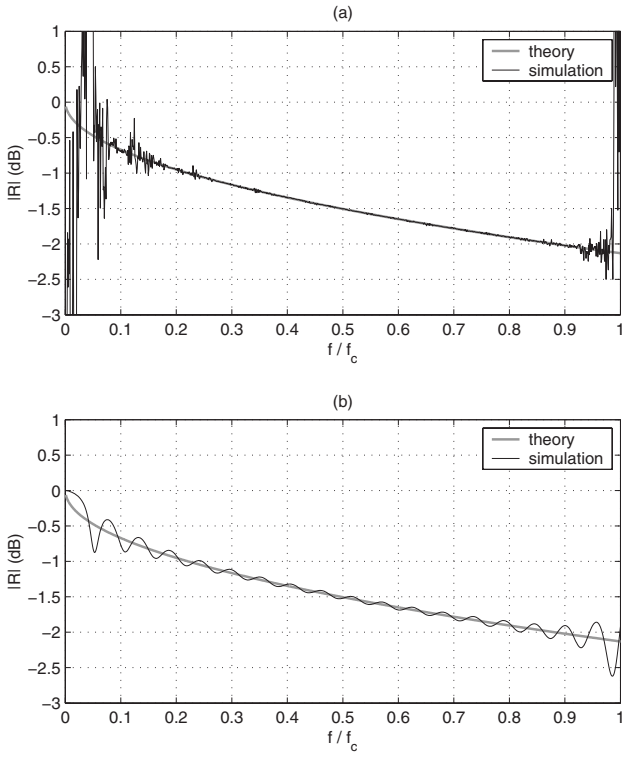

Figure 5. Reflection coefficient magnitude of the cylindrical tube. In the simulation, errors are artificially introduced. (a) Independent noise signals were added to the microphone signals. (b) The lengths of the calibration tubes were slightly altered.

data. As explained in section 2.3, random (noise) and systematic (calibration) errors can occur with the measurement method. In this section, computer simulations with a very basic model of the acoustic vibrations in the measurement set-up are used to study the effects of noise and calibration errors. In the model, the relationship between the microphone signal ratio and the impedance load Z at the reference plane is defined by the theoretical "plane wave" (PW) formulations in equations (19) and (20). The calibration procedure is simulated by calculating the microphone signals for the known loads of the four calibration tubes, using a theoretical expression for the propagation constant [27]. Next, the microphone ratio is calculated for a $128\,\mathrm{mm}$ long cylindrical tube with closed end and of the same cross-section as the measurement duct, and the impedance is obtained using equation 8. Of course, this simulation procedure gives perfect, error-free answers unless errors are intentionally added.

In order to study the effect of noise errors, white noise was added to the simulated microphone signals. The microphone distance was taken as $d = 7\,\mathrm{mm}$ (microphone combination I). As explained in section 2.4, that means accurate results can be obtained at frequencies in the range $[0.3 - 0.8]f_c$, where $f_c = c/(2d) \approx 24.6\,\mathrm{kHz}$ is the first singular frequency. Figure 5a shows the effects on the reflection coefficient versus f/f_c. As expected from the theory explained in section 2.3, the noise effects are strong at frequencies near 0 and near f_c. Importantly, the results are hardly affected by the noise in the region $[0.3 - 0.8]f_c$.

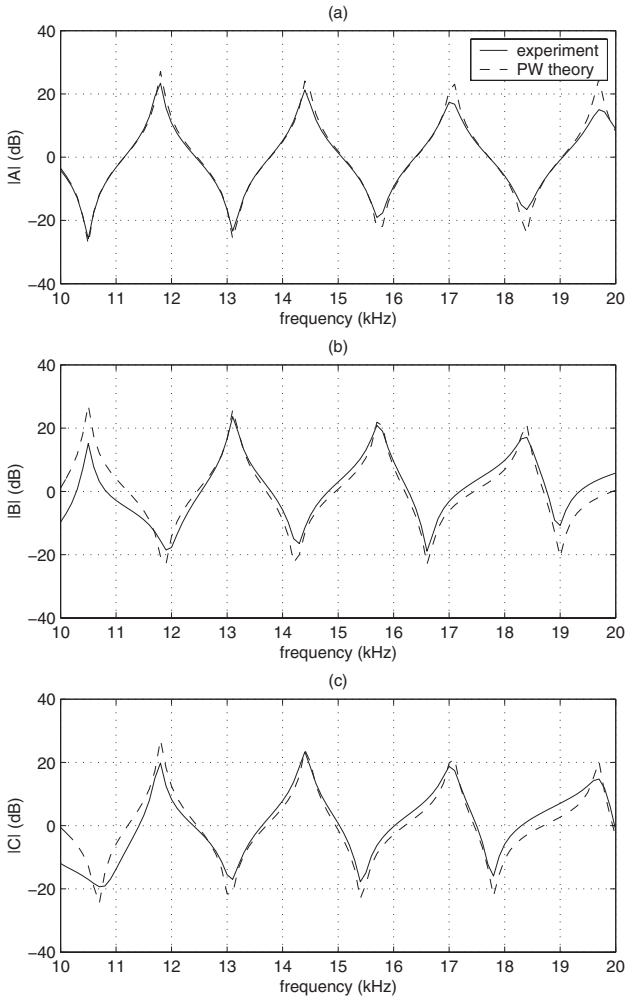

Figure 6. Calibration coefficients, as determined experimentally using microphone combination I. (a) Magnitude of A. (b) Magnitude of B. (c) Magnitude of C.

The effects of calibration errors can be studied by altering the lengths of the calibration tubes by a small fraction. Figure 5b shows the reflection coefficient magnitudes obtained by off-setting the negative-length tube by $-0.1\,\mathrm{mm}$, and the positive- and double-length tube by $+0.1\,\mathrm{mm}$. An oscillation appears in the simulated curve; the period of oscillation is related to the effective length of the tube under study. As with noise errors, the effects are larger near the singularities and the middle range.

Interestingly, the effects of noise and calibration errors are independent of the distance x_1 between the reference plane and the first microphone. That is, the simulations give identical results when varying x_1 but keeping d constant. Hence the choice of x_1 is not critical with the TMFC method.

3.2. Calibration coefficients

Precise determination of the calibration coefficients A, B, and C is vital for accurate measurement of the impedance of the object under study. Figure 6 shows the coefficient magnitudes, as determined at frequencies between 10 and $20\,\mathrm{kHz}$, using $d = 7\,\mathrm{mm}$ (microphone combination I). For

comparison, the values of the coefficients according to PW theory (equations 21, 22, and 23 with $G = 1$), are also shown.

between theory and experiment is relatively good for coefficient A. This is mainly because, as can be seen from equation 21, A depends only on how the pressure p_1 experienced by the diaphragm of the first microphone relates to the pressure and volume flow at the reference plane; it does not depend on how p_1 relates to the microphone signal s_1 (i.e. the microphone transducing characteristics H_1), nor on any properties related to the second microphone. The diminished extrema are due to non-propagating modes excited at the microphone positions.

The match between theory and experiment is less good for the coefficients B and C. The increased deviations are partly caused by the difference in transducing characteristics between the two microphones; in principle this can be corrected for by pre-calibrating the microphones. Further deviations are due to the effects of non-propagating mode excitation, and also due to the small cross-sectional discontinuity that waves travelling between the second microphone and the reference plane experience when passing the first microphone, which causes added reflections of waves. The experiments we conducted show that the nature and magnitude of these further deviations are very sensitive to the way the microphones are placed into their positions. Switching the two microphones indicated that these effects are not negligible in comparison with microphone transducing differences.

In conclusion, the calibration results show the limit for high frequencies of calibration methods that involve PW approximations, such as the method by Chung and Blaser [8], and indicate the necessity of using a calibration method that takes into account not only the microphone transducing characteristics, but also the effects they have on the acoustic field inside the tube.

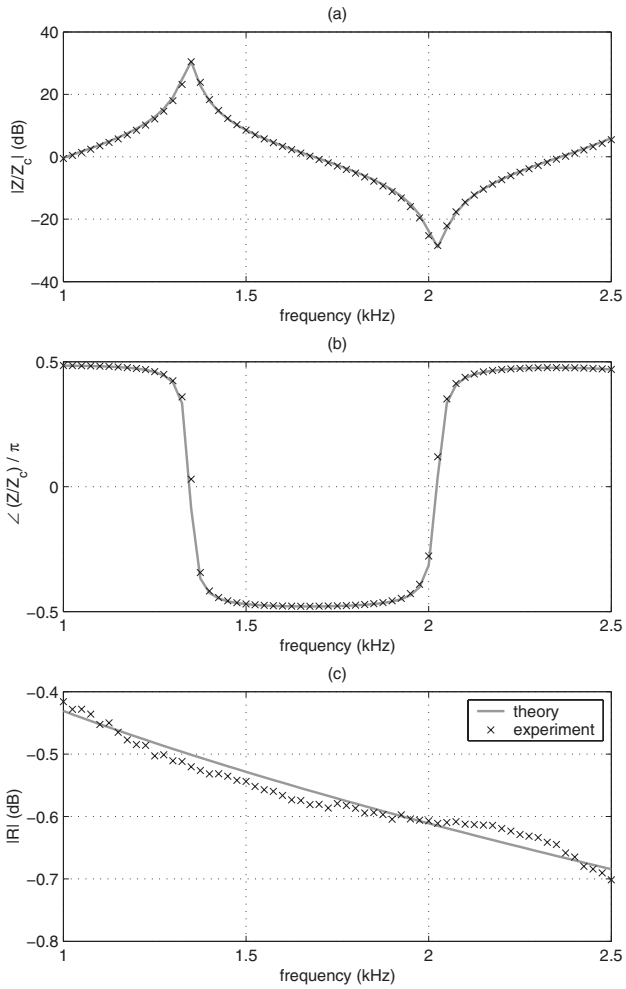

Figure 7. Response data measured with the short cylindrical tube of equal cross-section, using microphone combination VI. (a) Impedance magnitude (normalised). (b) Impedance phase. (c) Reflection coefficient magnitude.

3.3. Short cylindrical tube of equal cross-section

For testing the accuracy of the method, one needs to measure an object of which the impedance is known with relatively high certainty. For the TMFC method, the most suitable test object is probably a cylindrical tube with closed end and a cross-section that is exactly equal to that of the measurement duct. In our experiments we used a tube of 128 mm length.

Figures 7, 8, 9, and 10 show the measurement results obtained with microphone combinations VI, IV, II, and I, respectively. The total frequency range at which the impedance of the test tube is measured is 1 to 20 kHz. Each of the four figures shows the magnitude and phase of the normalised impedance, and the reflection coefficient magnitude (in dB). As can be seen from the plots, the errors are most easily observed in the latter quantity. This is because for cylindrical tubes, R varies over a much smaller dynamic range than $\bar{Z}$.

At the lower frequencies (1 to 5 kHz), the measured reflection coefficient magnitude is within 0.05 dB of the theoretical curve. At frequencies above 5 kHz, the deviation in measured reflection coefficient magnitude gradually increases towards about 0.2 dB near 20 kHz.

In principle, it is possible to merge the results shown in figures 7, 8, 9, and 10 in order to obtain a complete set of response data between 1 and 20 kHz. One must then however take care in ensuring that the individual measurement sessions are carried out under the same conditions. In particular, it is important to keep the temperature constant over the period of four measurement sessions. In order to ensure a smooth transistion between sets of results obtained with different microphone distances, the large-bandwidth result can be computed using a weighting function, such as applied by Vorländer [28].

From the reflection coefficient magnitude curves, it can be seen that the measurement errors are primarily structural, i.e. they exhibit oscillatory rather than noisy patterns. However, the size of the error exceeds that of what is predicted from the length-precision of the calibration tubes. The simulation results in section 3.1 showed that for length deviations of about 0.1 mm in the calibrations tubes, we may expect errors of less than 0.1 dB in the op-

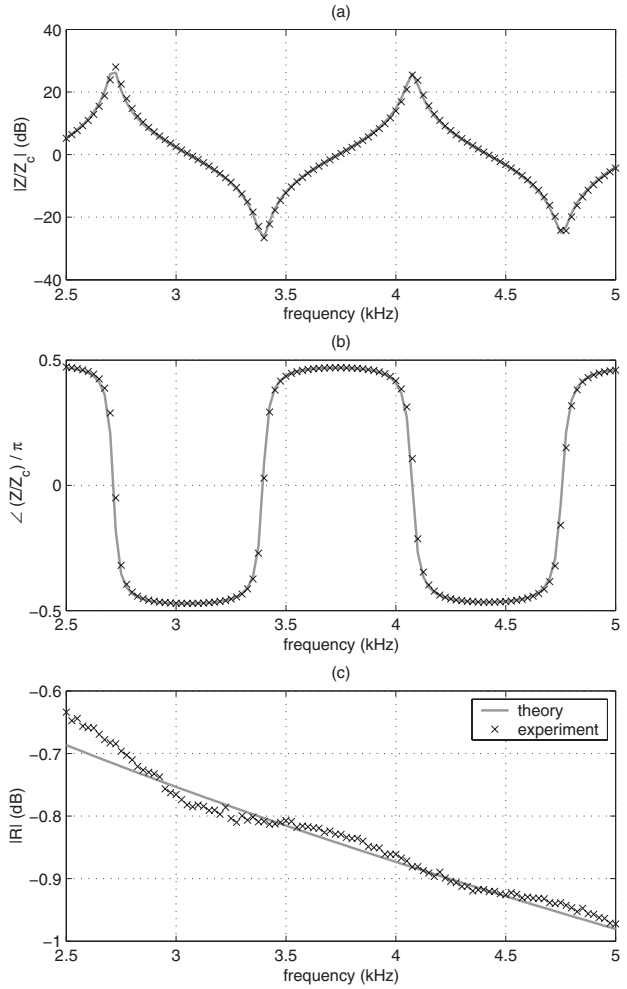

Figure 8. Response data measured with the short cylindrical tube of equal cross-section, using microphone combination IV. (a) Impedance magnitude (normalised). (b) Impedance phase. (c) Reflection coefficient magnitude.

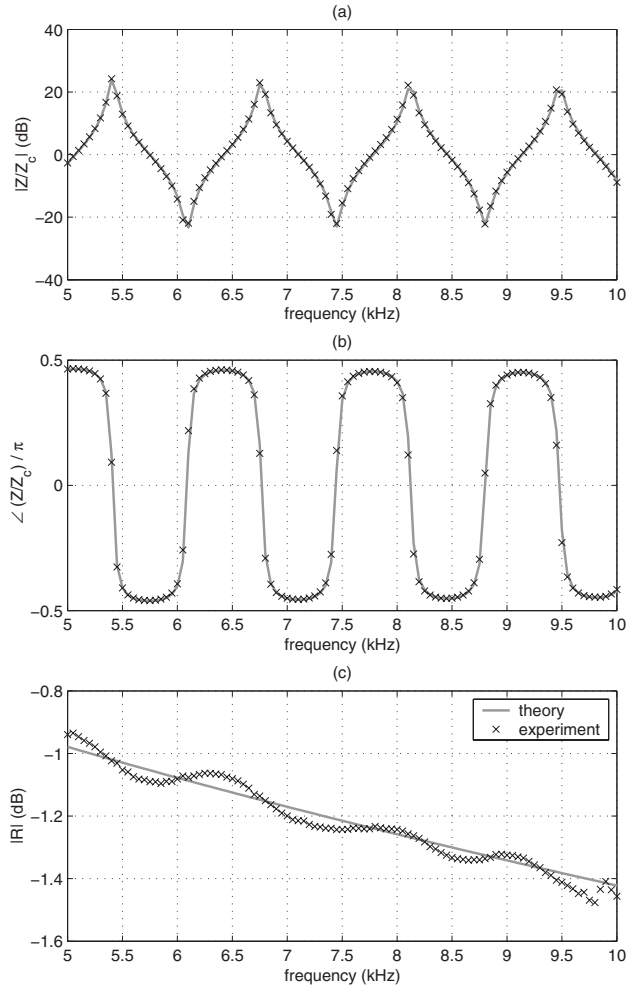

Figure 9. Response data measured with the cylindrical tube of equal cross-section, using microphone combination II. (a) Impedance magnitude (normalised). (b) Impedance phase. (c) Reflection coefficient magnitude.

timal frequency range when measuring a tube of 128 mm length. The actual calibration tubes have been measured to be more precise in length than 0.1 mm, but nevertheless errors larger than 0.1 dB can be observed at frequencies between 10 and 20 kHz. Furthermore, the nature of the error is different too; the oscillatory patterns are not as regular. This indicates that the structural errors are at least partly due to factors other than errors in the lengths of the calibration tubes. The most likely factors are other geometrical imperfections, such as small cross-sectional irregularities. Unlike with length imperfections - that can be defined as occurring at one specific point along the path of propagation of waves - these can occur over the complete length of a tube and are therefore more difficult to observe or measure, or to systematically incorporate in a model for error prediction such as in section 3.1. Improving the measurement apparatus with respect to cross-sectional irregularities would essentially require more sophisticated size-measuring tools than the ones that were available to the authors. Non-linearities could be another cause of structural errors, but are unlikely since measurements are carried out at low amplitudes, and no evidence of non-linear behaviour was found in the FFT-spectra of the microphone signals.

3.4. Plane Wave Attenuation

For studying the attenuation of plane waves in cylindrical ducts, a tube of 404 mm length was measured. The losses can be observed in the reflection coefficient magnitude, and are a function of the length and the attenuation constant. The attenuation constant is the real part of the propagation constant, and can be determined from the reflection coefficient using the formula:

$$\alpha = -\frac{log\,|R|}{2L}. \tag{31}$$

The oscillating curves in Figure 11 show the attenuation constant as a function of frequency, as deduced directly from the reflection coefficient of the long cylindrical tube measured at frequencies between 1 and 20 kHz. The results obtained with several different measurements sessions and microphone combinations are plotted. It is

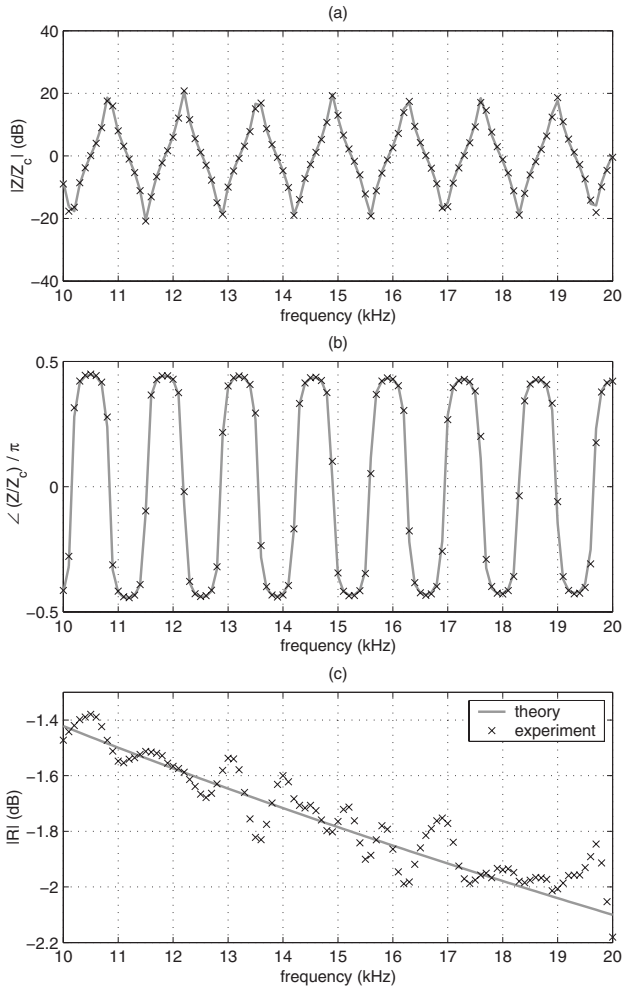

Figure 10. Response data measured with the short cylindrical tube of equal cross-section, using microphone combination I. (a) Impedance magnitude (normalised). (b) Impedance phase. (c) Reflection coefficient magnitude.

known from theory that attenuation is a monotonically increasing function of frequency [22]. It therefore makes sense to fit a smoothly rising function to the data, in order to make an estimate of the attenuation constant that is free of the spurious oscillations due to calibration errors. To this end, a function of the type

$$\alpha_f = c_1\sqrt{(\omega)} + c_2\,\omega^2 + \\ + \frac{c_3\,\omega^2}{1 + c_4\,\omega^2} + \frac{c_5\,\omega^2}{1 + c_6\,\omega^2} \qquad (32)$$

was fitted to the data; the form of equation 32 follows from theory (see Appendix A1).

For comparison, the attenuation constant as calculated from theory, and its decomposition into the attenuation α_w associated with viscothermal processes at the wall and the attenuation $(\alpha_c+\alpha_m)$ associated with classical and molecular effects, are also plotted. In various previous studies, that were restricted to lower frequency ranges [16, 17], the losses associated with classical and molecular effects have been neglected. As can be seen from Figure 11, this would result in a significant underprediction at the higher

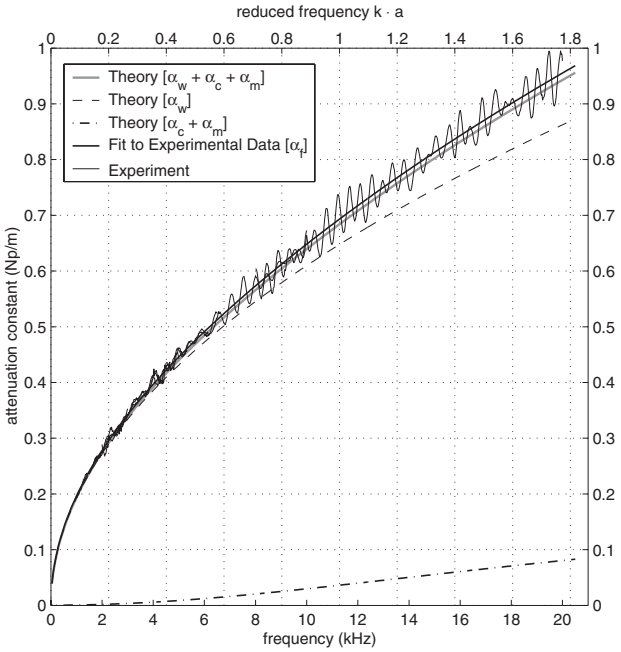

Figure 11. The attenuation coefficient, as deduced from the response data measured with the long cylindrical tube of equal cross-section. The results obtained with 6 different microphone combinations are plotted.

frequencies. The discrepancy between the fitted curve α_f and the theoretical curve is less than 1.4% at all frequencies up to 20 kHz. These results are comparable to those obtained by Dalmont [17], who measured a discrepancy of less than 3% at frequencies up to 5 kHz.

3.5. Cylindrical tube of different cross-section

As mentioned in section 2.5, the impedance derived using equation 8 does not always represent the impedance that is the objective of the measurement. In the case where the object under study has an entry cross-section that does not match the measurement duct cross-section, the derived impedance is the planar mode impedance $Z^{(1)}_{0,0}$ as calculated on the input side of the reference plane, whereas the input impedance of the object under study equals the planar mode impedance $Z^{(2)}_{0,0}$ on the object side of the reference plane. Under certain circumstances, explained in section 2.5, the relationship between these two planar mode impedances can be described with equation 29, derived from multimodal theory.

In order to test this theory, a tube with closed end of larger cross-section (18.7 mm in diameter and 239 mm in length) was connected to the measurement duct, and the impedance $Z^{(1)}_{0,0}$ was determined in the usual way. Microphone combination II was used, and frequencies between 5 and 10 kHz were measured. The impedance $Z^{(2)}_{0,0}$ was then computed using equation 29, with the number of higher modes taken into account set to $N = 40$. Figure 12 compares these impedances to the theoretical input impedance of the cylindrical tube. As expected, the impedance $Z^{(1)}_{0,0}$ does not match the theoretical impedance. The impedance

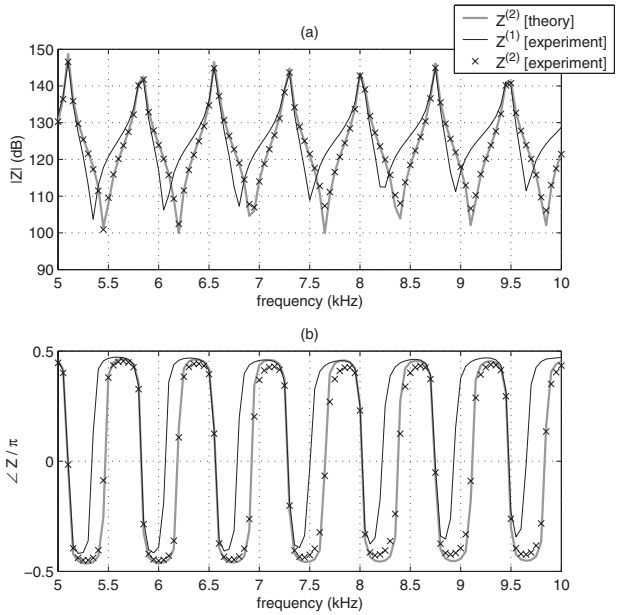

Figure 12. Response data measured with the cylindrical tube of different cross-section, using microphone combination II. (a) Impedance magnitude. (b) Impedance phase.

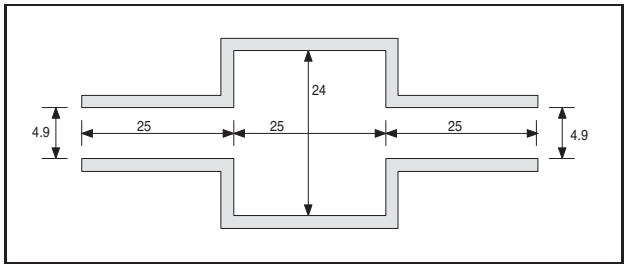

Figure 13. Dimensions of the expansion chamber (in mm). In both the experiments and the theoretical calculations, the object was terminated anechoically.

$Z^{(2)}_{0,0}$ approximates theory much more closely. However, the discrepancy between theory and experiment is larger than in the case of measuring a tube of equal cross-section; the impedance magnitude curves differ by more than 2 dB at some frequencies. This is probably because classical and molecular losses were not taken into account in the multi-modal model[3].

3.6. Expansion chamber

In order to test how experimental results compare with those obtained from multimodal theory, the impedance of the expansion chamber depicted in Figure 13 was measured. The entry cross-section of this object matches that of the measurement duct, thus we may directly derive the input impedance. Computations with the discrete-segment model of multimodal computation, as developed by Pagneux et al. [19] and recently elaborated by Kemp [4], indicated that for this tubular object the second mode is strongly excited in the wider part of the object.

[3] The higher-order mode theory of Bruneau *et al.* [27] was used for including boundary layer effects in the model.

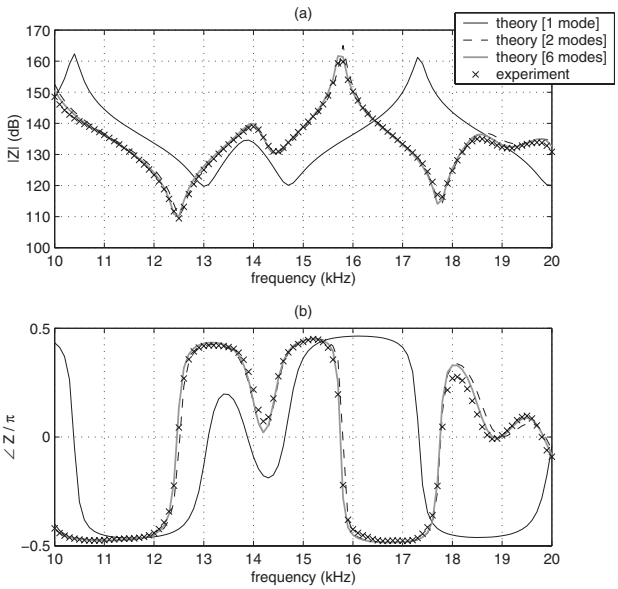

Figure 14. Response data measured with the expansion chamber, using microphone combination I. (a) Impedance magnitude. (b) Impedance phase.

Figure 14 shows the impedance of the expansion chamber. The measured impedance is compared to the impedance computed taking into account 1, 2, and 6 modes. The measured curve matches rather well with the curves computed taking into account 2 or more modes. The discrepancy between taking into account 1 or 2 modes is particularly striking in this case. This emphasises the need for the inclusion of at least one higher mode in the theoretical model.

4. Conclusions

A new method for calibrating a measurement set-up with two microphones fitted in a cylindrical measurement duct has been presented. A major advantage in comparison with many previous methods, such as the TMTC method, is that it does not require knowledge of the propagation constant. The calibration is completely general for a given constant temperature, and is relatively insensitive to ambient noise. The effects of non-propagating modes excited at the microphone positions and other influences related to the microphones are automatically calibrated out. The range of tubular objects that can be measured is not restricted to tubes that have the same cross-section as the measurement duct; a method based on multimodal theory has been proposed to take into account the effects of non-propagating modes at the discontuinuity at the reference plane in cases where the object has a different cross-section. Accurate experimental results have been obtained up to 20 kHz, which is just below the cut-on frequency of the anti-symmetric (0,1) mode of the measurement duct.

The method has been applied to experimentally determine plane wave losses in a cylindrical tube. The measured attenuation constant has been shown to be within 1.4% of the coefficient predicted by theory that includes the contributions of boundary layer losses, classical plane wave losses, and molecular relaxation processes.

A good concordance between multimodal theory and experiments was found for a tubular object in which higher modes are strongly excited due to abrupt changes in cross-section. This result paves the way for improving methods for bore reconstruction of quickly varying tubular profiles from acoustic data, by incorporating the effects of higher modes.

Major efforts have been made in order to minimise structural errors due to geometrical imperfections in the calibration tubes. However, some errors in measured impedances remain, and are larger than and of a different nature from those predicted for small errors in the lengths of the calibration tubes. These errors can probably be reduced by using even more precisely manufactured tubes and tubular connections.

The main priority of the present study being the experimental study of impedance at high frequencies, the apparatus was designed to cover a range between 1 and $20\,$kHz; the method has not yet been tested for frequencies below $1\,$kHz. Note that in order to measure at lower frequencies, the apparatus will have to consist of tubes of larger dimensions. For example, to measure the impedance at $50\,$Hz, the optimal distance between the microphones is about $1\,$m.

Acknowledgement

The authors are very greatful to Joel Gilbert for fruitful discussions and to Jean-Pierre Dalmont for helpful comments. The authors also acknowledge and thank Vince Devine for the precise manufacturing of the calibration tubes and other parts of the apparatus. This work was carried out under E.P.S.R.C. grant no. GR/N33072/01.

Appendix

A1. Propagation constant in a cylindrical tube

The following thermodynamic constants are given by Keefe [21] for wave propagation in air:

$$\begin{aligned}
\rho &= 1.1769 \cdot (1 - 0.00335\Delta T)\,\mathrm{Kg\,m^{-3}},\\
\mu &= 1.846 \cdot 10^{-5}(1 + 0.0025\Delta T)\mathrm{Kg\,s^{-1}m^{-1}},\\
\gamma &= 1.4017(1 - 0.00002\Delta T),\\
P_r &= \sqrt{0.8410(1 - 0.00002\Delta T)},\\
c &= 3.4723 \cdot 10^{2}(1 - 0.00166\Delta T)\,\mathrm{m\,s^{-1}},
\end{aligned}$$

where ρ is the mean density, μ is the coefficient of viscosity, γ is the ratio of specific heats, P_r is the Prandtl number, and c is the wave velocity. These values are evaluated at $T_0 = 300^o K$ (26.85^oC), and are accurate within $\pm 10^o$K of that temperature. The temperature difference relative to T_0 is ΔT.

For propagation of plane waves in a sufficiently wide cylindrical duct, in which the boundary layers occupy only a very small fraction of the duct's cross-sectional area, the propagation constant can be written [22]

$$\Gamma = \mathrm{j}\left(\frac{\omega}{c}\right) + (1+\mathrm{j})\alpha_w, \tag{A1}$$

where α_w is the attenuation constant associated with viscous drag and heat conduction at the tube wall. Pierce [22] gives the value

$$\alpha_w = \frac{1}{a}\sqrt{\frac{\omega\mu}{2\rho c^2}}\left[1 + \frac{\gamma - 1}{\sqrt{P_r}}\right]. \tag{A2}$$

More complex formulations of α_w are available in the literature (For an overview, see Tijdeman [29]), but the difference with equation A2 is usually very small (typically within 1% at frequencies below $20\,$kHz).

In the derivation of equation A2, standard attenuation of plane waves in free-space, i.e. the "classical losses", have been assumed to be much smaller than the wall losses and therefore neglected. Moreover, molecular relaxation processes have not been taken into account. Therefore, equation A2 is only valid at low frequencies. For accurate prediction of the total attenuation of a plane wave travelling in a cylindrical duct at frequencies up to $20\,$kHz, both the classical and molecular effects have to be added to the wall losses [30]. For a tube of $5\,$mm radius, and frequencies between 1 and $20\,$kHz, the phase velocity is only marginally affected by these processes[4], thus the propagation constant can be written:

$$\Gamma = \mathrm{j}\left(\frac{\omega}{c} + \alpha_w\right) + (\alpha_w + \alpha_c + \alpha_m). \tag{A3}$$

Pierce [22] gives formulae for the attenuation constants associated with classical (subscript c) and molecular (subscript m) effects:

$$\alpha_c = \frac{\omega^2\mu}{2\rho c^3}\left[\frac{4}{3} + \frac{\mu_B}{\mu} + \frac{\gamma - 1}{P_r}\right], \tag{A4}$$

$$\alpha_m = \sum_\nu \frac{(\alpha_\nu \lambda)_m}{\lambda}\,\frac{2\omega\tau_\nu}{1 + (\omega\tau_\nu)^2}, \tag{A5}$$

where $\mu_B \approx 0.6\mu$ is the bulk viscosity, $\lambda = c/f$ is the wavelength, and ν indicates the type of gas molecule. For air, which consists for 21% of O_2 ($\nu = 1$) and for 78% of N_2 ($\nu = 2$), the relaxation times are [22]

$$\tau_1 = \frac{1}{2\pi\,(24 + G)}, \tag{A6}$$

$$\tau_2 = \sqrt{\frac{T}{T_1}}\left\{\frac{1}{2\pi\,[9 + (3.5 \times 10^4)\,h\,\mathrm{e}^{-F}]}\right\}, \tag{A7}$$

[4] Dispersion associated with classical and molecular processes is small for large values of $s = a\sqrt{\rho\omega/\mu}$ [30].

where

$$G = (4.41 \times 10^6)\, h \left(\frac{0.05 + 100h}{0.391 + 100h} \right), \tag{A8}$$

and

$$F = 6.142 \left[\left(\frac{T_1}{T} \right)^{1/3} - 1 \right], \tag{A9}$$

with $T_1 = 293.16^o$K. The value h indicates the humidity factor:

$$h = \frac{0.01\,(RH)\,p_v}{p}, \tag{A10}$$

where p is the pressure (approximately equal to the atmospheric pressure at small oscillations), RH is the relative humidity (expressed as percentage) and p_v is the vapor pressure of water, which depends on the temperature. A third-order polynomial fit to the values given by Pierce (page 555) gives:

$$p_v = 0.065773\,t^3 + 0.1445\,t^2 + 59.34\,t + 560.54, \tag{A11}$$

where t is the temperature in ^{o}C. The term $(\alpha_\nu \lambda)_m$ in equation A5 represents the maximum absorption per wavelength associated with the ν-type relaxation process, and is given by:

$$(\alpha_\nu \lambda)_m = \frac{\pi}{2} \left(\frac{c_{v\nu}}{R} \right) \frac{(\gamma - 1)^2}{\gamma}, \tag{A12}$$

where $c_{v\nu}$ is the specific-heat contribution from internal vibrations of ν-type molecules, and R is the gas constant for air. The values of $(c_{v\nu}/R)$ for O_2 and N_2 are given by Pierce (page 554) for a number of temperatures between -10 and 40^oC. The following formulas are derived as third-order polynomial fits to these values:

$$\left(\frac{c_{v1}}{R} \right) \approx [-0.000002778\,t^3 + 0.0007857\,t^2 + 0.08599\,t + 3.883] \times 10^{-3}, \tag{A13}$$

$$\left(\frac{c_{v2}}{R} \right) \approx [-0.00000009259\,t^3 + 0.00035596\,t^2 + 0.02212\,t + 0.5525] \times 10^{-3}. \tag{A14}$$

The attenuation constants associated with classical and molecular effects are compared to the attenuation constant associated with wall losses for $a = 5$mm and $a = 10$mm in Figure A1.

A2. Impedance relationship at a cross-sectional discontinuity

For convenience, we repeat equation (28), which relates the impedances matrices on either side of the reference plane in Figure 4:

$$\mathbf{Z}^{(1)} = \mathbf{F}\mathbf{Z}^{(2)}\mathbf{F}^t. \tag{A15}$$

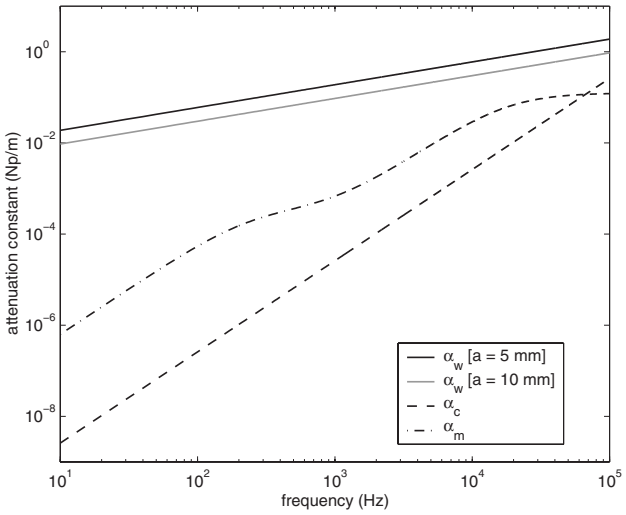

Figure A1. Attenuation constants versus frequency for sound in a pipe at 25^{o}C and 20% relative humidity.

If the non-propagating modes excited at the discontinuity are not coupled to any modes active in the rest of the object, the object impedance load as seen from the right-hand side of the reference plane equals that of an anechoic termination for all modes except the planar mode. The matrix $\mathbf{Z}^{(2)}$ is thus identical to the characteristic impedance matrix, except for the corner-element:

$$\mathbf{Z}^{(2)} = \begin{bmatrix} Z^{(2)}_{0,0} & 0 & \cdot\cdot & \cdot \\ 0 & Z^{(c)}_{1,1} & \cdot\cdot & \cdot \\ \cdot & \cdot & \cdot\cdot & \cdot \\ \cdot & \cdot & \cdot\cdot & \cdot \\ \cdot & \cdot & \cdot\cdot & Z^{(c)}_{N,N} \end{bmatrix}. \tag{A16}$$

The product of the first two terms in equation A15 is thus

$$\begin{bmatrix} F_{0,0}Z^{(2)}_{0,0} & F_{0,1}Z^{(c)}_{1,1} & \cdot\cdot & F_{0,N}Z^{(c)}_{N,N} \\ F_{1,0}Z^{(2)}_{0,0} & F_{1,1}Z^{(c)}_{1,1} & \cdot\cdot & \cdot \\ \cdot & \cdot & \cdot\cdot & \cdot \\ \cdot & \cdot & \cdot\cdot & \cdot \\ F_{N,0}Z^{(2)}_{0,0} & \cdot & \cdot\cdot & F_{N,N}Z^{(c)}_{N,N} \end{bmatrix}. \tag{A17}$$

The full product in equation A15 can be worked out; it is easily seen that the corner-element of this product is

$$Z^{(1)}_{0,0} = \mathbf{V}_1 \mathbf{V}_2^t, \tag{A18}$$

where

$$\mathbf{V}_1 = \begin{bmatrix} F_{0,0}Z^{(2)}_{0,0} & F_{0,1}Z^{(c)}_{1,1} & \cdot\cdot & F_{0,N}Z^{(c)}_{N,N} \end{bmatrix}, \tag{A19}$$

and

$$\mathbf{V}_2 = \begin{bmatrix} F_{0,0} & F_{0,1} & \cdot\cdot & F_{0,N} \end{bmatrix}. \tag{A20}$$

Thus, given that $F_{0,0} = 1$ [19, 4], we have

$$Z^{(1)}_{0,0} = Z^{(2)}_{0,0} + \sum_{n=1}^{N} (F_{0,n})^2 Z^{(c)}_{n,n}, \tag{A21}$$

which is equivalent to equation 29.

References

[1] J. P. Dalmont: Acoustic impedance measurement, Part I: a review. Journal of Sound and Vibration **243** (2001) 427–439.

[2] N. Amir, U. Shimony, G. Rosenhouse: Discrete model for tubular acoustic systems with varying cross section - the direct and inverse problems. Part I: Theory. Acta Acustica **81** (1995) 450–462.

[3] D. B. Sharp: Acoustic pulse reflectometry for the measurement of musical wind instruments. Dissertation. Department of Physics and Astronomy, University of Edinburgh, 1996.

[4] J. A. Kemp: Theoretical and experimental study of wave propagation in brass musical instruments. Dissertation. University of Edinburgh, 2002.

[5] W. Kausel: Bore reconstruction from measured acoustical input impedance; equipment, signal processing, algorithms and prerequisites. Proc. 2001 Int. Symposium on Musical Acoustics, Perugia, Italy, 2001, The Musical and Architectural Acoustics Laboratory FSSG-CNR, Venezia, Italia., 373–378.

[6] A. F. Seybert, D. F. Ross: Experimental determination of acoustic properties using a two-microphone random-excitation technique. J. Acoust. Soc. Am. **61** (1977) 1362–1370.

[7] A. F. Seybert: Two-sensor methods for the measurement of sound intensity and acoustic properties in ducts. J. Acoust. Soc. Am. **83** (1988) 2233–2239.

[8] J. Chung, D. Blaser: Transfer function method of measuring in-duct acoustic properties. I. theory. J. Acoust. Soc. Am. **68** (1980) 907–913.

[9] J. Chung, D. Blaser: Transfer function method of measuring in-duct acoustic properties. II. experiment. J. Acoust. Soc. Am. **68** (1980) 914–921.

[10] W. T. Chu: Extension of the two-microphone transfer function method for impedance tube measurements. J. Acoust. Soc. Am. **80** (1986) 347–348.

[11] W. T. Chu: Transfer function technique for impedance and absorption measurements in an impedance tube using a single microphone. J. Acoust. Soc. Am. **80** (1986) 555–560.

[12] W. T. Chu: Further experimental studies on the transfer-function technique for impedance tube measurements. J. Acoust. Soc. Am. **83** (1988) 2255–2260.

[13] H. Boden, M. Abom: Influence of errors on the two-microphone method for measuring acoustic properties in ducts. J. Acoust. Soc. Am. **79** (1986) 541–549.

[14] M. G. Jones, P. E. Stiede: Comparison of methods for determining specific acoustic impedance. J. Acoust. Soc. Am. **101** (1997) 2695–2704.

[15] B. F. G. Katz: Method to resolve microphone and sample location errors in the two-microphone duct measurement method. J. Acoust. Soc. Am. **108** (2000) 2231–2237.

[16] V. Gibiat, F. Laloë: Acoustical impedance measurements by the two-microphone-three-calibration (tmtc) method. J. Acoust. Soc. Am. **88** (1990) 2533–2544.

[17] J. P. Dalmont: Acoustic impedance measurement, Part II: a new calibration method. Journal of Sound and Vibration **243** (2001) 441–459.

[18] N. H. Fletcher, T. D. Rossing: The physics of musical instruments. Springer-Verlag, New York, 1991. Second Edition: 1998.

[19] V. Pagneux, N. Amir, J. Kergomard: A study of wave propagation in varying cross-section waveguides by modal decomposition. Part I: Theory and validation. J. Acoust. Soc. Am. **100** (1996) 2034–2048.

[20] D. H. Keefe: Woodwind air column models. J. Acoust. Soc. Am. **88** (1990) 35–51.

[21] D. H. Keefe: Acoustical wave propagation in cylindrical ducts: Transmission line parameter approximations for isothermal and nonisothermal boundary conditions. J. Acoust. Soc. Am. **75** (1984) 58–62.

[22] A. D. Pierce: Acoustics - an introduction to its physical principles and applications. Acoustical Society of America, New York, 1994.

[23] M. Bruneau: Introduction aux théories de l'acoustique. Université du Maine Editeur, Le Mans, 1983.

[24] M. O. van Walstijn, D. Campbell: Measurement of the acoustic response of a wind instrument with application to bore reconstruction. 144rd Meeting of the Acoustical Society of America, 2002, 2291.

[25] Y.-B. Jim, Y.-H. Kim: A measurement method of the flow rate in a pipe using a microphone array. J. Acoust. Soc. Am. **112** (2002) 856–864.

[26] S. Jang, J. Ih: On the multiple microphone method for measuring in-duct acoustic properties in the presence of mean flow. J. Acoust. Soc. Am. **103** (1997) 1520–1526.

[27] A. M. Bruneau, M. Bruneau, P. Herzog, J. Kergomard: Boundary layer attenuation of higher order modes in waveguides. Journal of Sound and Vibration **119** (1987) 15–27.

[28] M. Vorländer: Acoustic load on the ear caused by headphones. J. Acoust. Soc. Am. **107** (2000) 2082–2088.

[29] H. Tijdeman: On the propagation of sound waves in cylindrical tubes. Journal of Sound and Vibration **1** (1974) 1–33.

[30] J. Kergomard: Comments on "wall effects on sound propagation in tubes". Journal of Sound and Vibration **98** (1985) 149–155.